Data-driven classification of spectral profiles reveals brain region-specific plasticity

Christina Lubinus[1], Joan Orpella[2], Anne Keitel[3], Helene Gudi-Mindermann[4], Andreas K. Engel[5], Brigitte Röder[4], Johanna M. Rimmele[1,5,*]

Running title: Region-specific spectral plasticity

[1]Department of Neuroscience
Max-Planck-Institute for Empirical Aesthetics
Grüneburgweg 14
D - 60322 Frankfurt am Main, Germany

[2]Department of Psychology
New York University
6 Washington Place
New York , NY 10003, USA

[3]Department of Psychology
University of Dundee
Scrymgeour Building
Dundee DD1 4HN, Scotland, UK

[4]Biological Psychology and Neuropsychology
University of Hamburg
Von-Melle-Park 11
D - 20146 Hamburg, Germany

[5]Department of Neurophysiology and Pathophysiology
University Medical Center Hamburg-Eppendorf
Martinistraße 52
D - 20246 Hamburg, Germany

Corresponding author:
Johanna M. Rimmele, PhD
Department of Neuroscience
Max-Planck-Institute for Empirical Aesthetics
Grüneburgweg 14
D - 60322 Frankfurt am Main, Germany
phone: +49 (69) 8300479-323
Email: johanna.rimmele@ae.mpg.de

Abstract

The human brain exhibits rhythms that are characteristic for anatomical areas and presumably involved in perceptual and cognitive processes. Visual deprivation results in behavioral adaptation and cortical reorganization. Whether neuroplasticity-related mechanisms involve altered spectral properties of neural signals and which brain areas are particularly affected, is unknown. We analyzed magnetoencephalography resting state data of congenitally blind and matched sighted individuals. First, using clustering procedures (k-means and Gaussian Mixture Models) we identified brain region-specific spectral clusters. Second, a classifier was employed testing the specificity of the spectral profiles within and the differences between groups. We replicated previously reported findings of area-specific spectral profiles, indicated by high classification performance in the sighted. Additionally, we found high classification performance in the blind, suggesting that area-specific spectral profiles were consistently identified after deprivation-related reorganization. Crucially, in the cross-group classification (sighted vs. blind), several sensory (visual and auditory) and right frontal areas were classified worse compared to the control (within sighted classification) condition. Overall the spectral profiles of these areas showed increased neuronal power in higher frequency bands in the blind compared to the sighted, possibly reflecting acceleration of regionally prevalent brain rhythms. The spectral profiles in areas where group differences were observed correlated with microstructural white matter properties in an extended posterior and bilateral cluster. We provide evidence that visual deprivation-related plasticity particulary alters the spectral profiles of right frontal, visual and auditory brain regions, possibly reflecting increased temporal processing capabilities (auditory, frontal cortices) and changes in the visual inhibitory-excitatory circuits in the blind.

Introduction

Congenital blindness is associated with adaptive behavior and neural reorganization. Congenitally blind individuals (CB) show behavioral advantages in a range of different auditory (e.g. pitch discrimination (1), sound localization (2,3), voice recognition (4,5), or temporal order processing (6,7)), tactile (e.g. temporal order processing (6,8)) and higher-level cognitive tasks (e.g. auditory (9) and verbal memory (10,11); temporal attention (12), musical meter perception (13,14), temporal order verbal working memory (15), or the perception of ultra-fast speech (16–19), when compared to normally-sighted controls.

These behavioral changes have been related to observations from neuroimaging studies, which revealed altered structural and functional cortical properties. In particular, the occipital cortex of congenitally blind humans has been found to be characterized by decreased surface and volume of primary and visual association areas (20,21) and by increased thickness (22,23). Furthermore, visual areas have been found to be activated during various non-visual tasks in the congenitally blind, which is referred to as cross-modal plasticity (15,22–26). Visual deprivation-related cortical plasticity, however, is not restricted to the visual system as cortical reorganization was observed in the intact auditory (27) and somatosensory (28) cortices as well, reflecting intramodal plasticity (29). Additionally, functional magnetic resonance imaging (fMRI) in congenitally blind humans has revealed altered functional interactions of visual cortex with other cortical areas (24,30–34).

Whether the observed behavioral and neuronal changes in congenital blindness are accompanied by changes in the spectral properties of brain areas is largely unknown. Brain rhythms occur ubiquitously across the cortex (35–37), and specific spectral profiles seem to be associated with different anatomical areas (38,39). Brain rhythms most likely reflect the synchronization (phase-alignment) of oscillatory activity across neuronal populations, subserving the formation of both local assemblies and large-scale functional networks (40,41) through dynamical linking of brain areas into coherent functional networks for specific tasks (41–43). Various studies have observed that brain rhythms are recruited in a task-specific manner during perceptual, cognitive and motor

tasks (40,44–53). For example, theta-gamma brain rhythms was found to support episodic sequence memory in a visual task (53). Previous research has suggested that ongoing activity recorded during resting state to some extend reflects brain rhythms recruited during task-specific performances (38,42,54–57). Thus, beyond studying default mode network activity (57), resting state measurements are useful to study intrinsic brain rhythms of brain areas and to relate them to functional roles of these areas during task performance as shown using fMRI (58), magnetoencephalography (MEG) (38,59), electroencephalography (EEG) (39,43).

In congenitally blind individuals, the observation of a reduced or absent visual alpha rhythm is well-established (60–64). Only a few studies, however, have investigated the spectral power of brain areas and functional networks in the CB beyond alpha oscillations and beyond the visual cortex. One MEG study found increased connectivity in the delta and gamma ranges within visual cortex in the CB (63). Interestingly, despite the reduction in visual alpha power, the alpha connectivity between visual cortex and other cortical areas was preserved (Note, however, that the alpha band in this study was defined as a broader frequency band including traditional alpha and beta bands, 8-20 Hz). A study on sound categorization found that auditory and visual areas were more strongly connected in the blind, as measured by correlations of gamma-band power localized to these sensory areas (65), providing support for the notion of the visual cortex being incorporated into the intact sensory systems carrying out non-visual tasks. Furthermore, recent studies reported increases in beta-band connectivity involving visual cortex in the CB (15,26). Taken together, these results support the hypothesis that spectral properties are altered due to sensory deprivation, whereas the systematics (i.e., which brain areas and which spectral bands are affected) of these changes are unknown.

Here, we employed and extended a novel analysis pipeline (Fig 1), introduced by Keitel and Gross (38), to reveal differences in brain rhythms across spectral frequencies and cortical brain areas between CB and S. We hypothesized, first, that spectral profiles are region specific in sighted adults, enabling the classification of brain regions based on the spectral profiles. Second, we hypothesized that within a homogenous group of CB individuals, similar as in the sighted, spectral profiles follow specific patterns and enable the classification of brain regions, irrespective of eventual blindness-related

changes. Third, visual deprivation-related plasticity was predicted to result in altered spectral profiles in the CB compared to the sighted, particularly for brain regions for which visual deprivation-related reorganization has previously been shown, such as for sensory cortices. Our analysis pipeline was capable to overcome limitations of standard analyses of brain rhythms, such as facing a predominant activity of frequencies in the alpha and super-low frequency ranges (1/f) and performing poorly at capturing the brains' temporal dynamics over the course of the recording session (41,59). The pipeline disentangled spectral properties in the lower frequency ranges using segment-based clustering (of source-localized Fourier spectra). The temporal dynamics of the spectral properties were captured by computing clusters across temporal segments of the MEG signal and, thus, taking the time course of activity into account. The pipeline further comprised a classifier analysis, which aimed to identify brain regions by their own spectral profile, thereby testing the regional specificity of spectral fingerprints.

Results

All analyses were carried out for three experimental groups: First, in order to replicate that spectral profiles are brain region-specific, a sighted group, instructed to maintain eyes open and fixate their gaze during the recording (S-EO; N = 23), was tested. Second, to test whether similar regionally specific spectral profiles exist in congenitally blind humans, resting MEG data of congenitally blind individuals (CB; N = 26) was analyzed. Crucially, whether there were differences in the spectral profiles between sighted and blind was assessed by comparing the region-specific spectral profiles of the CB to those of the group of sighted individuals when they were blindfolded (S-BF; N = 24), CB and sighted individuals were matched in age, gender and education. Following the pipeline proposed by (38), the following analyses were implemented (for an overview see Fig 1; details in the methods section): Fourier spectra were calculated for the preprocessed and segmented (0.8 s long trials) resting state MEG data, projected into source space and spectrally normalized. To localize region-specific spectral clusters, the brain was parcellated into individual regions of interest (ROI, N = 115) according to the Automated Anatomical Labeling (AAL) atlas (66). Single-subject and group-level clustering was applied (k-means (67) and Gaussian Mixture Modelling, GMM (68)), resulting in homogenous group-level spectral clusters for single ROIs. The

specificity of the spectral fingerprint of an ROI was assessed by a classifier approach, which identified single-subject anatomical regions (of one half of the group) by their spectral clusters based on group-level clusters from the other half of the group. To this end, first, an experimental group (e.g., the S-EO) was split into a training and a test set. Second, region-specific spectral clusters were calculated for the subjects in the training group. Third, the similarity between the calculated group-level clusters (training set) and individual 1st-level clusters (test set) was assessed by computing the probability (negative log-likelihood) of the test-group data given the training model. Thus, we obtained a fit between each individual anatomical region and all 115 brain areas (expressed in probabilities), which were ranked yielding ranks from 1 (best predictor region) to 115 (worst predictor region). This fitting procedure was repeated 1000 times. For the comparison of the S-BF and the CB group (cross-group condition), the S-BF individuals were used as the training group and the classification performance for the CB individuals were assessed.

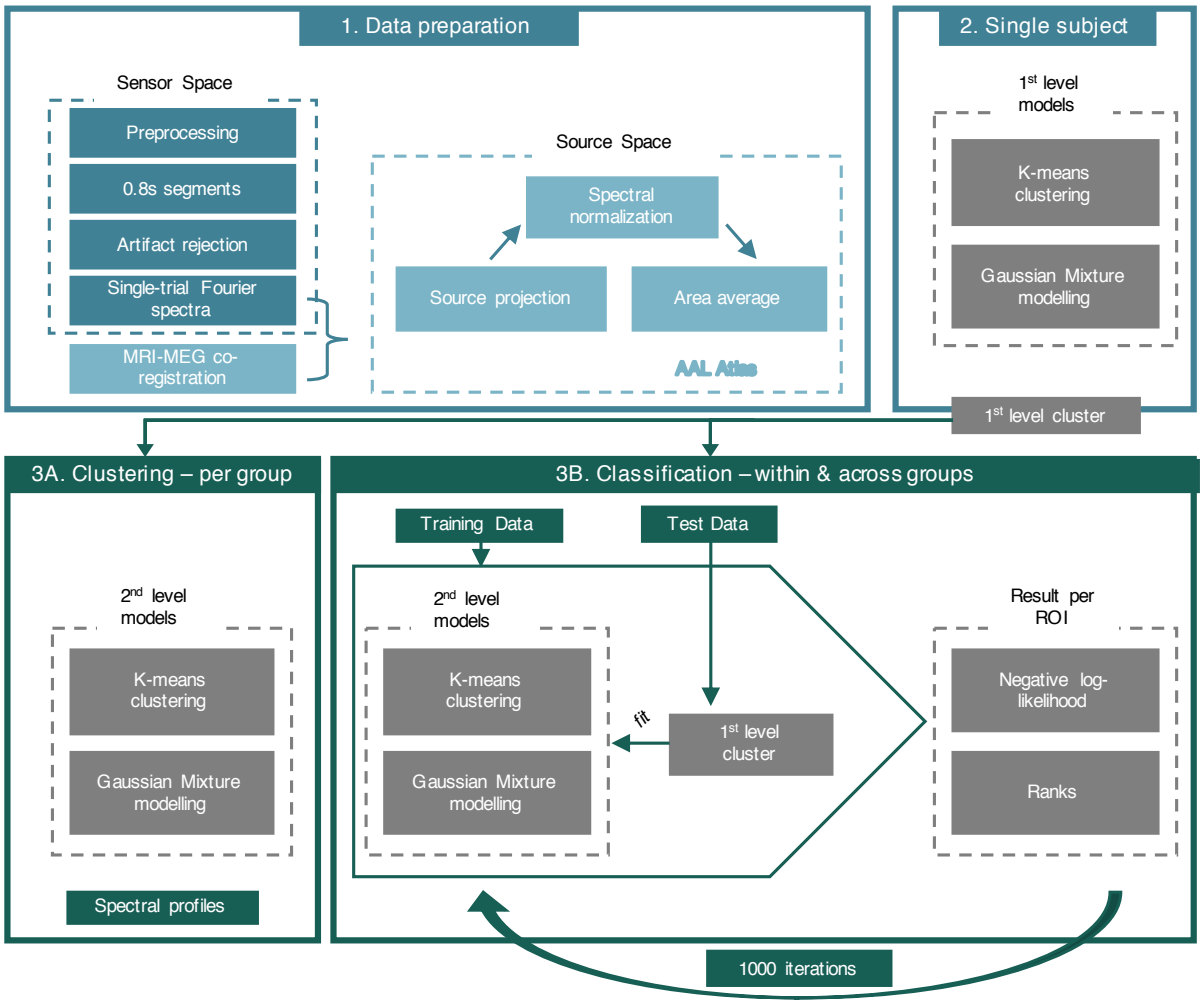

Fig 1. Analysis pipeline (adapted from (38)). (1) Continuous resting state MEG data were preprocessed and segmented into trials of 0.8 s length. Complex Fourier spectra were computed for each trial separately and projected into source space using previously defined beamforming (LCVM) coefficients. The data was spatially normalized, dividing each voxel's power by the mean power of all trials and voxels. Voxels were grouped according to the AAL atlas and power values were averaged across voxels of each anatomical area (N = 115). (2) In the 1st level analysis, power matrices were clustered into 9 distinct spectral clusters per participant and brain region using k-means and Gaussian Mixture model algorithms. (3A) In the 2nd-level analysis, 1st-level individual clusters were again subjected to k-means clustering and GMMs to establish region-specific spectral clusters consistent at the group level, also referred to as spectral fingerprints. The optimal number of group-level clusters per anatomical area were defined by the Silhouette Criterion prior to the group-level clustering procedure. (3B) For the classification procedure the experimental group was divided into training and test set. For each brain region, the fit between 1st-level clusters of the test group and group-level clusters of all regions of the training set was calculated. For each anatomical region, this resulted in a negative log-likelihood value for all regions (i.e. 115 values per region), indicating its similarity to all brain regions based on the spectral clusters. This fitting procedure between training and test set was repeated 1000 times with new group assignment (training vs test) on each iteration. The interindividual variance within test and training groups of each iteration was controlled for with additional 100 iterations within the respective sets.

Spectral fingerprints replicate

In our sample of sighted adults with open eyes we successfully replicated the classification of individual brain regions by their spectral profiles as first reported by (38). Particularly, the mean classification performance, indicated by the classification ranks, was high (as reported in the Keitel and Gross study) (Fig 2). Classification ranks refer to the probability of a region to be identified by the classifier: For example a mean rank of 1 indicates that a region was correctly assigned (i.e., highest propability among all areas) on every iteration, a mean rank of 2 means that the assignment was correct in many but not all of the iterations (i.e., had the second highest propability among all areas). Here, the mean rank (averaged across all iterations and brain areas) obtained from the classifier analysis was 2.70 (range of ranks: 1 – 12.7, Keitel mean rank = 1.8), or 2.32 when considering identification of the homologue (left/right hemisphere) areas as a hit (Keitel homologue mean rank = 1.4). Mean ranks of all ROIs are depicted in the histogram and surface plot in Fig 2. We here statistically quantified the classification performance using permutation tests. The mean classification rank of an area (e.g., right calcarine) was tested against a distribution of classification ranks of all brain areas (except the current one, e.g., right calcarine) accumulated across all iterations (N = 1000). For an area with a characteristic spectral profile, classification between corresponding areas (e.g., right calcarine in training vs test set) should be best and, thus, fall above the 95th percentile of the generated null-distribution. This analysis revealed

that for 97% of all areas classification was significantly better when identifying themselves compared to all other regions.

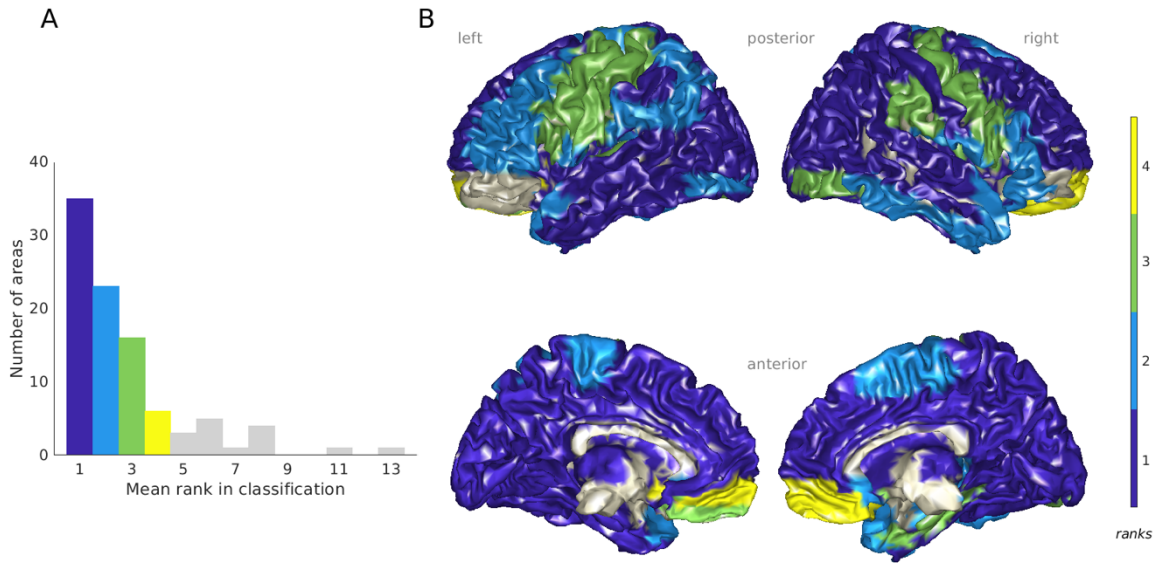

Fig 2. Classification results for the sighted with open eyes (replication sample). (A) Histogram of mean ranks in classification across all 115 brain areas. 84.5% of the brain regions obtain a mean rank between 1 and 4, while 15.5% of regions were assigned ranks up to 13. (in Keitel and Gross (38) all mean ranks were between 1 and 4), (B) Topography of mean ranks (colors match ranks from the histogram). Bin width is one for all subplots.

Furthermore – although the average optimal number of clusters (cf. methods) per anatomical area was lower in our sample (3.4 +/- 2.3 clusters per area (see Fig 5 and Fig S1) vs 4.1 +/- 1.86 (M + STD) in Keitel and Gross (38)) – the clustering approach revealed comparable spectral fingerprints between the studies. Interestingly, for deeper subcortical brain structures (e.g., thalamic and limbic areas) the clusters were less characteristic in the present data (i.e., only few clusters per area with less specific shapes and high classification ranks; see S1 Fig) – possibly reflecting limitations of the signal-to-noise ratio of the used MEG system.

Good classification within sighted and congenitally blind

Our second hypothesis stated that, within a group of congenitally blind individuals anatomical areas are characterized by specific (although possibly altered compared to the sighted) spectral fingerprints. We performed the classification procedure for the CB and observed good classification ranks (similar to the ones observed for the S-EO) (mean rank = 2.51, range = 1 - 10.3, homologue mean rank = 2.10, percent significant

ROIs = 100%), indicating consistent spectral clusters of brain areas in congenitally blind participants. The same procedure was performed on the data of the S-BF and revealed similarly good classification ranks (S-BF: mean rank = 2.64, range = 1-11.4, homologue mean rank = 2.17, percent significant ROIs = 98%) compared to the S-EO and CB.

Ensuring good within group classification in the CB and the S-BF was an important prerequisite for consecutive between-group analyses because it reassured that potential group differences did not arise from large within-group variance. Furthermore, the results showed a similar distribution of mean ranks across the cortical surface for both the CB and the S-BF group.

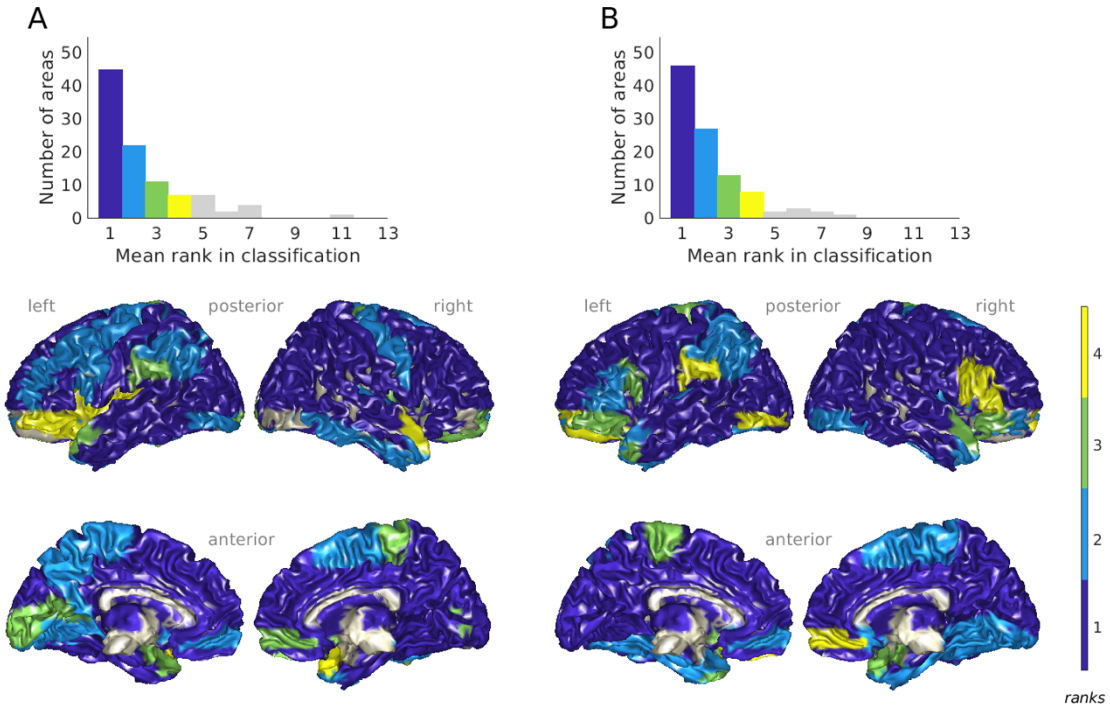

Fig 3. Classification results for the congenitally blind and the blindfolded sighted. (A) Sighted eyes closed. (Upper) Histogram of mean ranks in classification across all 115 brain areas. (Lower) Topography of mean ranks (colors match ranks from histogram). (B) Congenitally blind. (Upper) Histogram of mean ranks in classification across all 115 brain regions. (Lower) Topography of mean ranks (colors match ranks from histogram). Bin width is one for all subplots.

Spectral changes in sensory and right frontal regions in the congenitally blind

Based on the literature on intra- and cross-modal plasticity and behavioral adaptation in the CB, we hypothesized that spectral properties may differ between the congenitally blind and normally sighted individuals. To test if (and which) brain areas differed in their

spectral properties between the two groups, we implemented a cross-group classification drawing samples from the S-BF for the training and samples from the CB for the test group. Thus, region-specific single-subject spectra in the CB had to be identified based on the group-level clusters of the S-BF. This analysis resulted in a mean rank of 5.3 (range = 1.09 - 27.17) (Fig 4A).

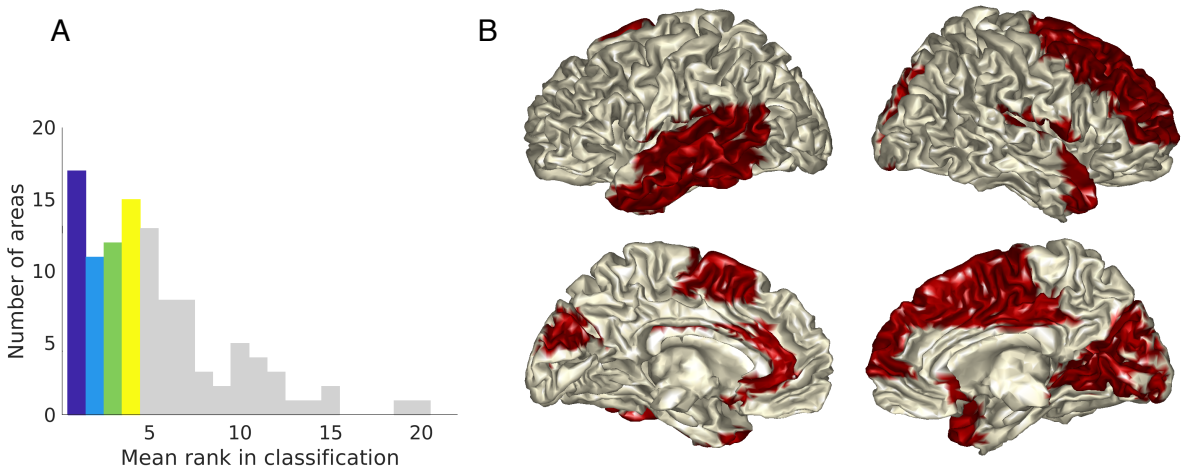

Fig 4. Cross-group comparison. (A) Histogram of classification ranks. Bin width is one. (B) The topographic distribution of significantly different classification ranks in the cross-group classification is highlighted in red, as tested by a permutation procedure.

In the cross-group analysis, 54.8% of 115 areas obtained classification ranks ranging from 1 to 4, while the automatic identification of the remaining regions was less precise (see Fig 4A). A visual inspection of mean rank values across areas and groups, i.e. S-EO, S-BF, CB, cross-group (see Table 1), revealed that some brain regions (i.e., precentral gyrus) obtained similar rank values for the within-group and across-group classification analyses, while the rank values increased (that is, classification accuracy decreased) for other areas (i.e., Heschl's gyrus, calcarine).

ROIs		**Mean ranks**			
Anatomical area	Side	S-EO	S-BF	CB	Cross-group
Calcarine gyrus	L	1.22	3.91	1,01	15.91
Calcarine gyrus	R	1.00	1.04	1,00	**11.45***
Heschl's gyrus	L	3.66	4.20	2,54	10.89
Heschl's gyrus	R	1.83	2.50	1,34	**12.40***
Postcentral gyrus	L	3.24	1.88	1,00	3.69

Postcentral gyrus	R	1.66	1.78	1,18	5.51
		S-EO	S-BF	CB	Cross-group
Sup. occipital gyrus	L	1.41	1.32	1,30	5.23
Sup. occipital gyrus	R	1.49	1.12	1,17	**5.70***
Sup. temporal gyrus	L	1.30	1.41	1,27	**12.40***
Sup. temporal gyrus	R	1.57	1.84	1,31	4.75
Precentral gyrus	L	3.33	2.17	1,45	3.36
Precentral gyrus	R	3.53	2.71	1,13	3.78

Table 1. Mean classification ranks for a selection of brain areas in primary and (extended) secondary sensory areas. S-EO, sighted eyes open; S-BF, sighted eyes blindfolded, CB, congenitally blind eyes blindfolded; sup., superior; *, brain areas showing significant group differences in the cross-group classification.

Beyond these descriptive procedures, we statistically compared classification results in the cross-group condition compared to the within S-BF group classification. In particular, this analysis assessed whether the mean rank of corresponding brain areas (e.g., calcarine-calcarine) between training (S-BF) and test (CB) sets differed from the classification ranks of the same region across all iterations (N = 1000) in the S-BF group. To this end, a distribution of ranks was generated from all iterations (N = 1000) of the fitting procedure for the S-BF group, against which the mean rank of the cross-group classification was tested; this was done separately for each ROI (see S2 Fig for the distributions of all brain areas). As seen in Fig 4B cross-group classification ranks were significantly worse for several sensory as well as for right frontal areas. This suggests that spectral profiles in sensory (e.g., right calcarine, right Heschl's gyrus, left superior temporal gyrus) and right frontal (e.g., right superior frontal gyrus) brain regions were different in the CB compared to the sighted, while no differences were found for other brain areas (see Table 2 for all ROIs showing significantly worse classification compared to the null-distribution).

Coarse region	**Hemisphere**	
	Left	**Right**
Frontal		Superior frontal gyrus
		Middle frontal gyrus
		Superior medial frontal
		Rolandic Operculum
Visual	Cuneus	Calcarine gyrus
		Cuneus
		Superior occipital gyrus

		Lingual gyrus
Temporal	Superior temporal gyrus Middle temporal gyrus Middle temporal pole Inferior temporal gyrus	Heschl's gyrus Middle temporal pole Superior temporal pole
Sensorimotor	Supplementary Motor Area	Supplementary Motor Area
Non-cortical	Olfactory Anterior cingulate cortex Cerebellum lobule VI Cerebellar vermis 3 Cerebellar vermis 9	Olfactory Middle cingulate cortex Cerebellum lobule X Cerebellar vermis 3 Cerebellar vermis 9

Table 2. Table of all brain areas (out of 115) for which classification ranks were significantly different between the congenitally blind and the sighted (both blindfolded).

Interestingly, the brain areas identified to show group-differences in the spectral profiles in the cross-group classification were characterized by clusters comprising peaks with increased power at higher frequencies in the CB compared to the S-BF participants (for a selection of brain areas with significant effects, see Fig 5A; spectra of all brain areas are shown in S1 Fig). This result pattern was observed for the auditory (with more power in the alpha and beta band in the CB compared to the sighted participants), and the right frontal areas (more power in the beta band). In visual brain areas, power peaks were reduced in the alpha band for the CB compared to the S-BF participants, however, power was increased in the low-gamma band. Post-hoc permutation tests were performed to confirm these observations. To test differences in spectral signatures between the S-BF and CB, the raw Fourier spectra (i.e. without applying the spectral clustering) were extracted und subjected to permutation statistics. Participants' group assignment (S-BF vs. CB) was permuted randomly (1000 permutations) ($Q = 0.05$; false discovery rate (FDR) corrected p-value = .033; p-values < .033) (Fig 5B and Fig S3). Note, that the differences in low-gamma power in the calcarine between the CB and the S-BF were not significant in the post-hoc tests.

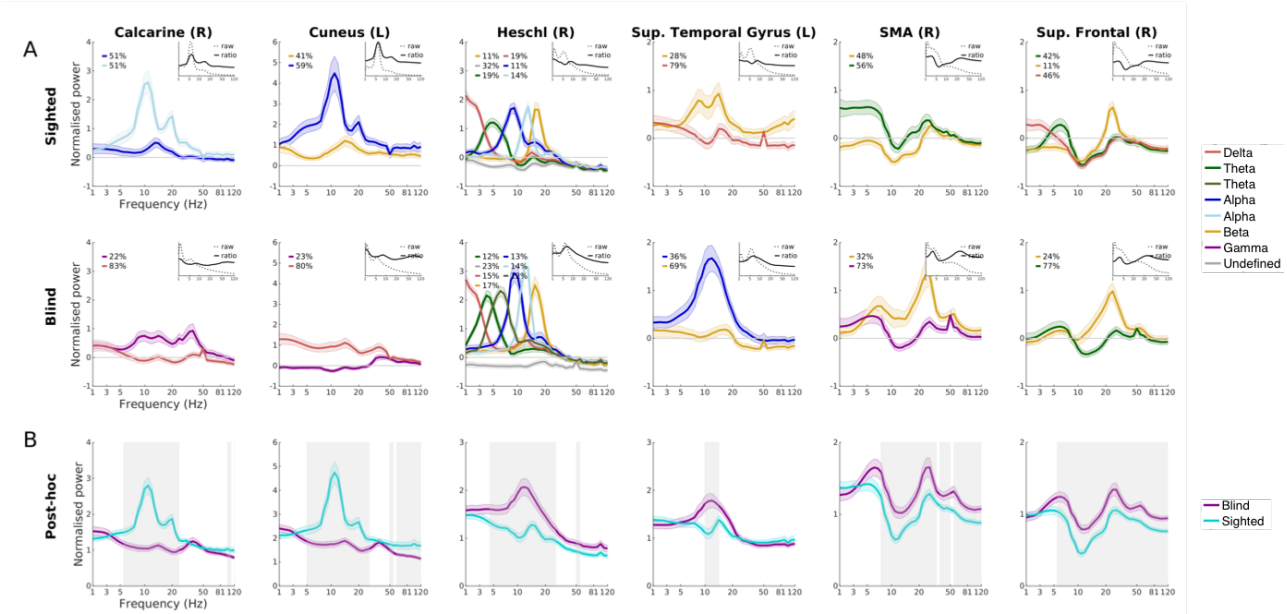

Fig 5. Comparison of spectral profiles of sighted and blind participants. (A) A selection of the spectral profiles of the brain areas (columns) that showed significantly worse cross-group classification is displayed, separately for the S-BF and the CB (rows). Clusters are color-coded according to the frequency of the cluster amplitude peak (legend on the right). The insets display the normalized mean power spectra (solid lines) and the unnormalized mean power spectra (dashed lines) (i.e. both without applying the spectral clustering). (B) Post-hoc analysis of the spectral differences are displayed for the selection of brain regions (columns). Spectra represent normalized mean power spectra (i.e. without applying the spectral clustering) at each ROI. Frequencies where power differences were obtained between the groups are highlighted in grey (permutation test: Q = 0.05; FDR corrected p-value = .033; p-values < .033). The groups are color-coded (legend on the right). In all panels: shaded lines indicate standard error of the mean.

Spectral changes correlate with structural group differences

In order to better understand the spectral differences between the groups observed in the classifier analyses and their relation to brain structure, we performed an exploratory diffusion-tensor imaging (DTI) data analysis for a subsample of participants. In particular, we used tract-based spatial statistics (TBSS) (69) to quantify white matter differences between the CB and sighted participants. The TBSS analysis revealed significantly higher Radial Diffusivity (RD) values in a bilateral posterior spatial cluster (i.e. a cluster of voxels) for the CB compared to the sighted participants ($N_{sighted}$ = 12, N_{CB} = 16; family-wise error (FWE)-corrected at the peak voxel, two-sided p = 0.05; S4 Fig B), indicating reduced white matter structural connectivity in the CB group. Individual RD values for this cluster were extracted and correlated with the raw normalized power spectrum of cortical brain areas that showed significant differences in the classifier analysis (17 areas). RD correlated negatively with the average power in right calcarine

gyrus (rho = -0.66, p = .00013), right ligual (rho = -0.58, p = .00136), right superior occipital gyrus (rho = -0.56, p = .00197), left (rho = -0.60, p = .00066) and right (rho = -0.60, p = .00071) cuneus, indicating that reduced white matter properties in occipital areas were accompanied by reduced neuronal power. RD correlated positively with the average power in: Heschl's gyrus (rho = 0.68, p = .00007), the superior (rho = 0.44, p = .01781) and middle (rho = 0.40, p = .03516) temporal pole, and right rolandic operculum (rho = 0.66, p = .00013) (S4 Fig A), indicating that reduced white matter properties in these areas were accompanied by increased neuronal power. Of these regions, the superior and middle temporal pole did not survive Bonferroni correction to control for multiple comparisons (α = .00294). The CB contributed strongest to the correlations (cf. S4 Fig A). The remaining regions (cf. methods section) showing significant group differences regarding their spectral clusters did not correlate with the RD values.

We finally used a probabilistic atlas of white matter pathways in MNI space (70) to evaluate the overlap of the spatial cluster with known white matter tracts. With the probabilistic atlas thresholded at 0.95, the TBSS cluster presents a significant overlap with the posterior corpus callosum, the posterior inferior longitudinal fasciculus (bilaterally), the posterior inferior fronto-occipital fasciculus (bilaterally), and the optic radiations (also bilaterally). This means that there is a 95% chance that the white matter abnormalities identified in the CB by the TBSS analysis primarily affect these white matter tracts.

Discussion

The present study provides new insights into region-specific spectral profiles across cortical brain areas and frequency bands in congenitally blind and sighted adults. We implemented a novel whole-brain analysis pipeline, adapted from (38), capable of disclosing temporally-resolved spectral clusters specific to individual brain regions. K-means clustering and GMM were employed to establish spectral patterns across trials and subjects in the three experimental groups (S-EO, S-BF, CB). A classifier automatically identified anatomical areas based on their spectral profiles separately for each group. Finally, a cross-group classification determined brain regions that were spectrally different in the blind and the sighted group. Our first main finding is that the clustering and classification procedures performed exceptionally well for all three groups

(97-100% of areas were classified correctly in each group). This highlights consistent brain area-specific spectral properties across individuals within the sighted and, as shown for the first time, within the congenitally blind group. Crucially, second, we showed that visual deprivation gave rise to changes in the spectral profiles especially of sensory (auditory and visual) and right-frontal cortical areas, as indicated by significantly worse classification performance in the cross-group comparison for these brain areas, but not for other brain areas. More specifically, the spectral profiles of these areas in the CB showed increased power in the alpha and/or beta frequency bands in the right primary auditory cortex and right-frontal brain regions compared to the sighted. The visual cortex in the CB was characterized by a cluster with decreased alpha power and a gamma (~40 Hz) peak, which was absent in the sighted. In addition to the observed spectral group differences, the averaged power in some of the spectrally-altered brain areas revealed correlations with microstructural white matter properties. Our findings suggest that visual deprivation alters spectral properties particularly of brain areas, which have been previously suggested to show functional and structural reorganization. Spectral power in these brain areas was altered in an area-specific manner, possibly reflecting anatomical reorganization and changes in the functionally-specific processes of these areas in the congenitally blind.

Robust classification of brain areas based on spectral profiles

Spectral clustering and automatic classification revealed spectral profiles, classification ranks and distributions of classification ranks across the cortex in the S-EO group similar to the ones first reported by (38). Spectral profiles, for example of occipital regions, showed the typically observed peak at ~10 Hz. Spectral peaks in the beta band (~20 Hz) were prominent across frontal and central brain areas, resembling previously reported natural frequencies of these brain areas (Fig 5; (38,71,72)). While the spectral profiles of most brain areas well resembled those reported by Keitel and Gross, for some brain areas the spectral profiles differed (see S1 Fig). This suggests that the used recording system and/or the tested sample of participants can influence the specific profiles of some brain areas more than others. A test on a large dataset across different recording sites (i.e. several 100 recordings) will be necessary to clarify which spectral modes generalize across individuals of a larger population. Importantly, within

our sample, the spectral profiles were consistent across individuals (i.e. only group clusters were reported where at least ~70% of participants and on average ~97% for the S-EO and ~94% for the S-BF group contributed to each of the group-level spectral clusters). Thus, the present results show the robustness of brain area-specific spectral profiles, suggesting that spectral profiles are characteristic properties of cortical regions.

Crucially, a novel finding of our study is that spectral clusters were consistent within the group of congenitally blind individuals as well (Fig 3B). Analogously to the sighted group, brain regions could be identified reliably based on their spectral clusters suggesting spectral consistencies across individuals (i.e., only group clusters were reported where at least ~69% of participants and on average ~95 % contributed to each spectral cluster). This result suggests, that adaptation of the cortex to visual deprivation leads to homogenously altered spectral fingerprints in congenitally blind individuals. The finding is in line with previous research, showing altered neuronal structures and activity in the congenitally blind based on group-level analysis (25,73–75).

In our study, deep sub-cortical brain areas (in contrast to what has been reported by Keitel and Gross (38)) were not classified well (S1 Fig). A possible explanation is a lower signal-to-noise ratio in deeper brain areas in our data compared to Keitel and Gross, due to the usage of different MEG systems.

Selective spectral plasticity across the brain

In the cross-group classification brain areas of individual CB participants were classified based on the group-level spectral clusters of the S-BF. In order to isolate visual deprivation-related effects, the participant groups were well matched in our study (cf. methods section). While in the cross-group classification, the classification for the majority of the brain areas was relatively good (i.e., low ranks; Fig 4A), spectra related to auditory, visual and right frontal regions, which are typically associated with deprivation-related intramodal and crossmodal changes (15,22–26,29), were classified significantly worse compared to the within-sighted classification (Fig 4B). Importantly, these findings suggest that the spectral properties of brain areas are not homogenously altered by deprivation-related plasticity. Previously, a non-monotonic relationship between plasticity and stability across cortex, with decreases in plasticity from early visual

to mid-level cortex and increases in plasticity higher in the visual cortical hierarchy, has been reported using fMRI (76, see also 77).

Spectral plasticity in sensory areas

Our findings highlight changes in spectral properties of auditory and visual cortex due to visual deprivation-related neuroplasticity. The findings confirm previous reports both demonstrating cross-modal reorganization in visual cortex (15,22–26) and intra-modal reorganization in auditory cortex (29) in blind humans. Our findings extend these reports by providing evidence for genuine changes in the processing mode of these regions, as indicated by changes in the spectral characteristics.

Visual brain areas classified as spectrally different between the sighted and the blind involved primary visual cortex (calcarine sulcus) and its adjacent areas (cuneus, lingual gyrus), as well as more dorsal (superior occipital gyrus) visual regions and parts of the ventral visual stream (left inferior temporal gyrus), involved in visual object recognition (78) (Table 2). In these areas, we observed one cluster with a clear visual alpha peak at ~10 Hz for the sighted, and a second alpha cluster characterized by a smaller amplitude (note that the two clusters are displayed by two separate lines in Fig 5A). Keitel and Gross (38) speculated that the second alpha cluster in the middle occipital gyrus (which was present ~80 % of the time) indicates continuous alpha suppression during visual fixation. Our findings show, however, firstly, that both clusters occur with a similar prevalence across time and, secondly, that the second alpha cluster is similarly present during eyes open (present ~60% (left) or ~55% (right) of the time) and eyes closed (present ~40% (left) or ~50% (right) of the time) conditions (Fig 5A (upper), S1 Fig). In contrast, in the CB these typically visual areas were characterized by a first cluster with a strongly reduced alpha power peak, shifted towards higher (beta, gamma) frequencies, as well as a second cluster with close to zero power in the alpha band (Fig 5A, B). This observation is in line with previous findings reporting a reduced or entirely absent alpha rhythm in the visual system in blind individuals (60–63). Interestingly, the spectral profile of one cluster in visual areas in the blind included a peak in the low-gamma (~40 Hz) range which was not present in the spectal profile of the sighted. This finding is in line with a recent report, which found enhanced gamma power correlations within visual cortex using MEG (63) in congenitally blind individuals.

The alpha rhythm in humans likely reflects a local mechanism of rhythmic inhibition (79) mediating top-down control by feedback connections (80) and controlling gamma-amplitude (81, see 82). Synchronized gamma activity - controlled by alpha (de-)synchronization and phase - is suggested to serve a feedforward function, processing sensory information (80,83). In light of this idea, our results suggest that the decreased alpha and increased gamma power in the blind reflect an altered excitation-inhibition balance in the visual system due to visual deprivation (82,84). While visual cortex is functionally inhibited during rest and with closed eyes in the sighted, feedforward visual cortex processing seems to be enhanced in the congenitally blind, presumably due to disinhibition (reduced/absent alpha rhythm) as consequence of atrophy in the thalamocortical connections. Higher visual cortex metabolism in the CB (85,86), might reflect the altered neuronal activity. Possibly, the lack of visual cortex inhibition in the blind (here observed during rest) is related to changes in the functional role of visual cortex during task-specific processing, i.e., an increased recruitment of visual cortex during the processing of non-visual tasks (25,73,75,87), whereas the specific mechanisms are unknown.

Additionally, we found altered spectral profiles in auditory cortex with increases in the power in specific frequency bands. Brain areas in temporal cortex that were identified by the classifier to be spectrally different between the sighted and blind involved primary auditory cortex (right Heschl's gyrus) and areas of the ventral auditory stream (bilateral middle temporal pole, right superior temporal pole, left middle temporal, superior temporal and inferior temporal gyri) (Table 2). In these areas, we observed increased power at higher frequencies (alpha to beta range) in the blind compared to the sighted (Fig 5A, B). Similarly, bilateral supplementary motor area similarly showed increased power in the beta band (and absence of delta- and theta-band peaks) in the CB compared to the sighted (S1 Fig). Interestingly, previous research on ultra-fast speech processing in congenitally blind individuals reported that enhanced comprehension of ultra-fast speech in the blind is accompanied by increased speech-tracking of higher frequencies in the alpha-beta range (16 Hz) in right auditory cortex (i.e., phase-alignment to the speech signal), compared to sighted individuals (19). Importantly, in a comparison of primary auditory cortex spectral profiles during rest and during speech comprehension, Keitel and Gross provided evidence for the functional

relevance of the delta, theta and beta brain rhythms for speech processing (38). A large amount of studies related temporal processing to the entrainment of auditory cortex oscillations (48,88–90). Thus, more generally, our findings of frequency increases of spectral power might be related to increased temporal processing abilities, as often reported for congenitally blind individuals (6–8,12,15,18,19,91). In line with these assumptions, on the other side of the plasticity spectrum, age related decline in processing fast speech has been related to a slowing of theta oscillations (92), additionally supporting the association of spectral dynamics within auditory cortex with temporal (speech) processesing.

Spectral plasticity in right frontal cortex

Beyond spectral reorganization in sensory cortices, our data suggest that particularly right-hemispheric frontal brain regions undergo adaptation as spectral clusters of right middle frontal and superior frontal gyri were significantly different between the blind and the sighted. Previous research on plasticity, has suggested that frontal cortex is particularly prone to reorganization (76,77). Interestingly, changes in lateralization of cognitive processes have been previously reported previously in congenitally blind individuals. The predominance of the widely distributed frontotemporal language network in the left hemisphere is a robust finding, shown across different languages (93), developmental stages (94) and linguistic tasks (93,95,96). In congenital blindness, however, language processing likely is reflected in a reduced left-hemispheric lateralization of the frontotemporal network (97,98). Although the spectral bands affected by the altered lateralization of language processing are unknown, interestingly, beta-band activity has been related to language processing (99). Thus, it is possible that the altered spectral profiles in the right-hemispheric frontal brain regions observed here reflect changes in the hemispheric lateralization of the frontotemporal language network in congenital blind adults.

Besides altered brain spectral profiles compared to the sighted, blind individuals showed compromised microstructural white matter integrity in visual association tracts comprising the ventral visual stream. These tracts included the bilateral inferior fronto-occipital fasciculus, connecting occipital and frontal brain areas, which supposedly is

related to reading, writing and language semantics (100); the bilateral inferior longitudinal fasciculus, connecting occipital and anterior temporal cortices, which plays a role in reading, language and semantic processing (100,101; S4 A Fig); and the bilateral optic radiations, linking the visual thalamus to the primary visual cortex. In addition, white matter integrity was also compromised in the posterior corpus callosum (by which homologous visual cortices are interconnected (102). Detoriation of the visual association tracts, which are related to visual, memory and language processing (101), as well as the optic radiations and visual callosal areas in congenitally blind individuals has been previously shown (102). Here, we observed that these structural changes in white matter integrity in the blind, correlated with alterations in the spectral profiles of visual cortex, auditory sensory processing areas and parts of frontal cortex (cf. S4 B Fig). In contrast, other areas that showed altered spectral profiles, e.g., the right superior and middle frontal or left middle temporal areas, did not correlate with the anatomical changes.Thus, the observed visual deprivation related changes in brain spectral profiles of some – but not all – brain areas were related to structural alterations.

One limitation of the present study is that the interpretation of group differences in the region specific spectral profile is complicated by the multidimensionality of the spectral profiles. For that reason, we additionally performed a post-hoc analysis of the non-clustered data (based on the averaged brain area spectrum) to evaluate the cross-group differences between the sighted and congenitally blind individuals (i.e., which frequencies show significant power differences; Fig 5B; results section). The analysis confirmed the findings from the spectral clustering approach.

Concluding remarks

The present study supports the findings of robust brain area-specific spectral profiles in the human brain. Crucially, we provide novel findings that suggest region specific alternations of these profiles in congenitally blind adults. An increase in higher frequency bands in auditory and frontal brain regions might be related to the higher termporal processing capacities in the blind while altered spectral profiles in visual brain regions might indicate a change in the excitation-inhibition balance.

Materials and Methods

Participants

The study was approved by the German Psychological Association. All participants gave written informed consent prior to the experiments and received monetary compensation. The data were recorded in the context of a larger project (15,26). Three to four minutes of resting state MEG data were collected from a group of sighted and congenitally blind individuals matched in age, gender and education. During data collection the CB and the sighted (S-BF) were blindfolded, however, for the sighted an additional resting state measurement with open eyes was conducted (S-EO). The data reported here include (after a few subjects were excluded, see below) 26 subjects for the CB (12 females; mean age: 37.8 years; SD: 10.2 years; age range: 22-55 years), 24 for the S-BF (11 females; mean age: 36.8 years; SD: 10.1 years; age range: 21-55 years) and 23 for the S-EO (11 females; mean age: 37.3 years; SD: 9.8 years; age range: 21-55 years). A few subjects had been excluded after data collection because of corrupted resting state files (one subject for the CB, one subject for the S-EO) or no individual structural MRI scan (three subjects for the S-BF and S-EO). All participants were healthy with normal hearing (self-report) and assured no history of psychiatric or neurological disorders. One blind participant reported a history of depressive mood disorder, but was free of symptoms and without current treatment. Sighted participants had normal or corrected to normal vision (self-report). In the blind, vision loss was total and resulted from a variety of peripheral (pre)natal conditions (retinopathy of prematurity: n=9; genetic defect, n=5; congenital optic atrophy: n=2; Leber's congenital amaurosis: n=2; congenital cataracts, glaucoma: n= 2; congenital retinitis: n= 2; binocular anophthalmia: n= 2; retinitis pigmentosa: n= 1; congenital degeneration of the retina, n=1). 17 participants reported minimal residual light perception.

MRI and MEG data acquisition

For all participants T1-weighted structural MRI scans and DWI-MRI scans were obtained with a 3T scanner (Siemens Magnetom Trio, Siemens, Erlangen, Germany). For the T1-weighted images we used the following parameters: TE = 2.98 ms, TR = 2300 ms, flip angle = 9, and isotropic 1 mm3 voxels, 256 sagittal slices. The MEG data

were recorded in a magnetically shielded room using a 275-channel whole-head system (Omega, 2000, CTF Systems Inc.), while participants sat in an upright position. The data were acquired with a sampling rate of 1200 Hz. Prior to each experiment, the head position was measured relative to the MEG sensors and during the recording the head position was tracked.

Data analysis

The initial analyses in this study are adopted from the analysis pipeline proposed by (38).The modifications of the analysis pipeline and the novel analysis will be stated in detail. All analyses were carried out using Matlab R2018a version (The Math Works Inc), the Fieldtrip Toolbox (version 20181104) and SPM12.

Data preparation in sensor space: preprocessing, artifact rejection, source localization

During preprocessing, the MEG signal was downsampled to 250 Hz, denoised and detrended. To better capture the dynamically changing spectral properties of the brain, the continuous signal was segmented into trials of 0.8 s. Trials were declared as noisy and excluded when their z-score was higher than 2. On average, 7 trials were excluded, resulting in a mean of 340.3 trials (STD= 34.7) per subject (S-EO: mean = 346.7, STD = 37.4; S-BF: mean = 336.8, STD = 34.2; CB: mean = 338, STD 33.2). Due to shorter recordings in the present study, trial duration was slightly shortened, relative to the 1 s duration used in Keitel and Gross (2016), to increase statistical power. MEG channels were labeled as noisy and rejected when the ratio between their noise level (in STD) and that of the neighboring sensors (in STD) exceeded a value of 0.5 ((Sensor STD - Neighbor STD) / Neighbor STD; mean number of excluded channels = 1.22, STD = 1.34). Finally, using independent component analysis (ICA), data was cleaned from heartbeat, eye blinks and eye movements related artifacts (components were identified based on their time-course, topography and variance across trials). To prepare the source projection of the Fourier spectra, beamformer coefficients were obtained. For this purpose, we applied co-registration of individual T1-weighted MRI scans and the MEG coordinate system, realignment, segmentation and normalization to Montreal Neurological Institute (MNI) space. A forward model was created

using a single-shell model and linearly constrained minimum variance (LCMV) beamformer coefficients (103) were calculated for the MEG time series for each individual voxel on the 10 mm regular grid.

Spectral analysis in sensor space

The analyses described in the following were performed for all three groups separately (CB, S-EO, S-BF). First, Fourier-spectra were calculated on 0.8 s long trials for each subject, using a multitaper approach (3 tapers) and zero-padding (length of 2 s). Second, using the previously computed LCMV coefficients, the complex Fourier spectra were projected into source space. Fourier spectra of individual voxels and segments were ratio normalized, i.e., divided by the mean power across all voxels and trials (see S4 Fig for the power spectra used for the normalization in all groups). This ratio normalization resulted in voxel-specific spectral properties with values above/below one highlighting the differences of a given voxel to the mean spectral power across all voxels separately at each frequency. All values were subtracted by 1 (leading to values above/below zero), to facilitate the identification of changes in power (de/increases).

k-Means clustering and Gaussian mixture modelling of source-localized spectral activity

To identify region-specific spectral clusters in the individual subject, the brain was parcellated according to the AAL atlas (66) (116 regions of interest, ROIs). For one anatomical region (cerebellum 3L), however, the interpolation between the AAL atlas and the source model was not successful. Thus, this region was excluded and all analyses are based on the remaining 115 anatomical areas. For each of the ROIs, voxels were grouped and power spectra were averaged across voxels. Clustering algorithms were employed to identify spectral clusters. First, trial-by-frequency matrices were subjected to a k-means algorithm (67) which established spectral clusters by partitioning the n observations (0.8 s temporal segments) into k clusters. For the 1st-level analysis, the k was set to 9, based on the Silhouette criterion evaluation (104). Second, for each subject and ROI, GMMs (68) were fitted to the 9 clusters obtained from the k-means analysis (1st-level GMM). Next, in order to identify the optimal number of clusters per brain region across all subjects for the 2nd-level group analysis, the 1st-level GMMs were evaluated using the Silhouette criterion. Silhouette values were computed for cluster

solutions in the range from 1 to 15, the fitting was repeated 1000 times. At the group level, k-means clustering was applied to the 1st-level clusters in order to disclose consistent patterns across subjects. The optimal number of clusters per brain area, as assessed by the Silhouette criterion evaluation (104), was used as k-parameter for the algorithm. As before, k-means results were fed into GMM revealing the final clusters per brain region (2nd-level GMM).

Clusters were considered for visualization only if they were reflective of the majority of participants. To facilitate reading of the spectral plots, group-level clusters were color-coded according to the frequency of the maximum amplitude of the cluster (peak frequency) (delta: 1-3.5 Hz, red; theta: 4-8 Hz, green; alpha: 8.5-12.5 Hz, blue; beta: 14-30.5 Hz, yellow; gamma: 33.5-100 Hz, magenta). Furthermore, we computed the relevance of each cluster per brain region by analyzing the amount of single subject trials during which a cluster was present. Group clusters (Fig 1, step 3) were traced back to single subject clusters and the amount of trials that contributed to a single subject cluster (Fig 1, step 2) was calculated and expressed as percentage. Percentages were averaged across subjects.

Automatic within group classification

A classifier was employed to test the specificity of region-specific spectral fingerprints. After splitting each group into half (training and test group), group-level clusters were calculated for the training group for all anatomical regions using k-means and GMM clustering. For each brain region and participant of the test group, the similarity of spectral profiles was assessed compared to all brain regions of the 2nd-level group clusters of the training group by computing the negative log-likelihood for all pairs of regions. This procedure, that is group assignment and classification, was repeated 1000 times (note that for the S-EO one subject was left out in every iteration to yield an even number of participants in training and test groups). On each iteration, an additional loop (N = 100) controlled for interindividual noise within a group by randomly drawing the adequate number of subjects (i.e., $N_{S\text{-}EO} = 11$, $N_{S\text{-}BF} = 12$, $N_{CB} = 13$) from the group with replacement, allowing a subject to enter multiple times or not at all. Put differently, within one iteration (N = 1000) each participant belonged to either the training or the test group. To account for individual differences, the group clusters were calculated

100 times choosing a different subset from the respective group each time and finally averaged to obtain a robust group estimate. Based on the mode of clusters identified per brain region in the 2nd-level cluster analysis, the optimal number of clusters for the classification analysis was k = 2. Likelihood values were ranked and averaged across iterations (20% trimmed mean). For further comparisons, only corresponding ROIs (e.g., how is the Heschl ROI in the test set ranked based on the training set Heschl ROI) were considered.

Additionally, to the descriptive report of the classification performance, here we tested whether a specific ROI (of the test set) was classified significantly better by the corresponding area of the training set, compared to all other 115 ROIs. This allowed us to exclude the possibility that classification performance was caused by unspecific effects – that is, generic fingerprints. To this end, each region's mean rank (averaged across iterations) was tested against a distribution of classification ranks generated from all other ROIs (null-distribution).

Automatic cross-group classification

Crucially, in order to identify differences in region-specific spectral properties between the CB and S-BF, we performed a cross-group classification. The same classification procedure was employed, however, the classifier was trained on one group (S-BF), while the other (CB) was utilized as the test set. As before, the classification procedure was repeated 1000 times, drawing a subset of N = 12 per group on every iteration. Importantly, the randomization of subjects chosen on each iteration was identical to the one used for the within group classification in the S-BF (this is the reason why N = 12, instead of using all subjects of both groups). Thus, differences in the classification, as reflected by the ranks, could not be caused by the training set per se. In order to understand whether some brain areas in the CB were not classified well based on the S-BF spectral profiles (i.e. whether the classification of brain regions was different in the cross-group condition compared to the within S-BF classification), we tested the cross-group classification mean ranks against the distribution of ranks from the same ROI from the S-BF group (here the null-distribution). The distributions were generated by taking the classification rank of a corresponding area from training and test set (i.e. Calcarine) across all iterations (see S2 Fig for the distributions of all brain areas). We

calculated the 95th percentile of the distribution and tested whether the cross-group mean rank of the current region fell above (significant) or below (not significant) this threshold.

To further assess the spectral profiles of brain areas that were significantly different in the cross-group classification, post-hoc permutation statistics were applied to the raw, normalized region-specific spectra (i.e., Fourier spectra without clustering procedure). The spectral analysis was calculated as in the main analysis (see above). For all significant brain regions seperately, power was averaged across voxels and segments, resulting in a single power value per frequency and per subject. Based on frequency by subject matrices for the CB and the S-BF, group differences in spectral power were tested against a distribution where the group assignment (CB vs. S-BF) was randomly permuted (N = 1000). To control for multiple comparisons, we used FDR (Q = 0.05).

Microstructural white matter properties

DW-MRI data were acquired together with T1-weighted structural scans described above. We used an echo planar imaging (EPI) sequence optimized for DWI-MRI of white matter covering the whole brain (64 axial slices; bandwidth = 1502 Hz/Px, 104 × 128 matrix, TR, 8,200 ms; TE, 93 ms; flip angle, 90°; slice thickness, 2 mm; voxel size, 2 × 2 × 2 mm3). The protocol comprised three acquisitions yielding a total acquisition time of 9 minutes 51 seconds. This resulted in a total of 120 diffusion-weighted volumes with six interleaved non-diffusion-weighted volumes (b values of 1,500 s/mm2). DWI-MRI scans were aquired from a subset of the original sample including 16 blind and 12 sighted participants.

DTI-MRI preprocessing and analysis. Diffusion data processing initially corrected for eddy current distortions and head motion by using FMRIB's Diffusion Toolbox (FDT; FMRIB Software Library; FSL 5.0.1; http://www.fmrib.ox.ac.uk/ fsl/; (105)). For a more accurate estimate of diffusion tensor orientations, the gradient matrix was rotated to correct for head movement, using the fdt_rotate_bvecs program in FSL. We then used the Brain Extraction Tool (106) for brain extraction, also part of the FSL distribution. Analysis continued with the reconstruction of the diffusion tensors using FSL's DTIFIT program. FA and RD maps for each participant were calculated using the eigenvalues extracted from the diffusion tensors. Note that FA maps are required in the early stages

of TBSS, that is, to compute the registrations to MNI standard space and subsequently create the diffusion skeletons. However, we focused our analysis on RD, as this is a more specific measure of diffusivity in white matter than FA or mean diffusivity. Indeed, although several factors can contribute to produce particular RD values, including the number of axons and axon packing and diameter, RD has been most consistently related to myelin content along axons, with increased RD values reflecting higher demyelination (107–110). In animal studies, directional measures such as RD, unlike summary parameters such as mean diffusivity or FA, provide better structural details of the state of the axons and myelin (111).

Voxel-based analyses of RD maps were performed with TBSS (69). Participants' FA maps (necessary to calculate the registrations to MNI standard space and create the RD skeletons) were registered to the FMRIB58_FA template (MNI152 space and 1 × 1 × 1 mm3) using the nonlinear registration tool (112). These registered FA maps were first averaged to create a mean FA volume. A mean FA skeleton was then produced, representing the centers of all white matter tracts common to all participants in the study. Each participant's aligned FA data were then projected onto this skeleton by searching for the highest FA value within a search space perpendicular to each voxel of the mean skeleton. This process was repeated for the RD maps by applying the transformations previously calculated with the FA maps. This resulted in individual RD skeletons for each participant. Finally, to assess white matter differences between CB and sighted participants, independent-samples *t*-tests were performed on the RD skeleton. Significant results are reported at FWE-corrected $p < 0.05$ using threshold-free cluster enhancement 12/7/19 12:09:00 AM(113) and a nonparametric permutation test with 5,000 permutations (114). Significant cluster results were averaged and a mean value per participant, reflecting individual microstructural differences, was obtained.

Spearman correlations were used to analyse the correlation between RD values (across groups) and the spectral profiles of brain areas that showed significant group differences in the cross-classification. More specifically, all cortical areas that showed significant differences between the CB and sighted in both, the cross-classifiaction and the post-hoc analysis, were included. For these areas, the raw normalized power spec-

tra, averaged over the frequency bands where significant group differences were observed (Fig 5), was retrieved and correlated with the RD values. Bonferroni correction for multiple comparisons across brain areas was applied (α = .00294).

For the mapping between RD values and the standard probabilistic atlases of white matter pathways, all voxels that differed significantly in RD values between the CB and sighted were included. We report only tracts that showed an overlap with these voxels, with the tracts from the probabilistic atlas thresholded at 0.95 probability.

Funding

This research was supported by the DFG (SFB936/B2/A3; TRR169/A1/B1) and by the Max-Planck-Institute for Empirical Aesthetics.

Acknowledgements

We want to thank Laura Gwilliams and Federico Adolfi for helpful methodological discussions and comments.

References

1. Gougoux F, Lepore F, Lassonde M, Voss P, Zatorre RJ, Belin P. Pitch discrimination in the early blind. Nature. 2004 Jul;430(6997):309–309.
2. Lessard N, Paré M, Lepore F, Lassonde M. Early-blind human subjects localize sound sources better than sighted subjects. Nature. 1998 Sep;395(6699):278–80.
3. Gougoux F, Zatorre RJ, Lassonde M, Voss P, Lepore F. A functional neuroimaging study of sound localization: visual cortex activity predicts performance in early-blind individuals. Raichle M, editor. PLoS Biol. 2005 Jan;3(2):e27.
4. Bull R, Rathborn H, Clifford BR. The voice-recognition accuracy of blind listeners. Perception. 1983 Apr;12(2):223–6.
5. Foecker J, Best A, Hoelig C, Roeder B. The superiority in voice processing of the blind arises from neural plasticity at sensory processing stages. Neuropsychologia. 2012 Jul;50(8):2056–67.
6. Roeder B, Roesler F, Spence C. Early vision impairs tactile perception in the blind. Curr Biol. 2004 Jan;14(2):121–4.
7. Stevens AA, Weaver K. Auditory perceptual consolidation in early-onset blindness. Neuropsychologia. 2005 Jan;43(13):1901–10.
8. Hoetting K, Roesler F, Roeder B. Altered auditory-tactile interactions in congenitllally blind humans: an event-related potential study. Exp Brain Res. 2004;159:370–81.
9. Roeder B, Roesler F. Memory for environmental sounds in sighted, congenitally blind and late blind adults: evidence for cross-modal compensation. Int J Psychophysiol. 2003 Oct;50(1–2):27–39.
10. Roeder B, Roesler F, Neville HJ. Auditory memory in congenitally blind adults: a behavioral-electrophysiological investigation. Cogn Brain Res. 2001 Apr;11(2):289–303.
11. Amedi A, Raz N, Pianka P, Malach R, Zohary E. Early 'visual' cortex activation correlates with superior verbal memory performance in the blind. Nat Neurosci. 2003 Jul;6(7):758–66.

12. Roeder B, Kraemer UM, Lange K. Congenitally blind humans use different stimulus selection strategies in hearing: An ERP study of spatial and temporal attention. Restor Neurol Neurosci. 2007;25:12.

13. Lerens E, Araneda R, Renier L, De Volder AG. Improved Beat Asynchrony Detection in Early Blind Individuals. Perception. 2014 Oct;43(10):1083–96.

14. Carrara-Augustenborg C, Schultz BG. The implicit learning of metrical and non-metrical rhythms in blind and sighted adults. Psychol Res. 2019 Jul;83(5):907–23.

15. Rimmele JM, Gudi-Mindermann H, Nolte G, Roeder B, Engel AK. Working memory training integrates visual cortex into beta-band networks in congenitally blind individuals. NeuroImage. 2019 Jul;194:259–71.

16. Hertrich I, Dietrich S, Moos A, Trouvain J, Ackermann H. Enhanced speech perception capabilities in a blind listener are associated with activation of fusiform gyrus and primary visual cortex. Neurocase. 2009 Apr;15(2):163–70.

17. Dietrich S, Hertrich I, Ackermann H. Ultra-fast speech comprehension in blind subjects engages primary visual cortex, fusiform gyrus, and pulvinar – a functional magnetic resonance imaging (fMRI) study. BMC Neurosci [Internet]. 2013 Dec [cited 2019 Feb 22];14(1). Available from: https://bmcneurosci.biomedcentral.com/articles/10.1186/1471-2202-14-74

18. Trouvain J, Trouvain P-B. On the comprehension of extremely fast synthetic speech. Saarl Work Pap Linguist. 2007;9.

19. Hertrich I, Dietrich S, Ackermann H. Tracking the speech signal – Time-locked MEG signals during perception of ultra-fast and moderately fast speech in blind and in sighted listeners. Brain Lang. 2013 Jan;124(1):9–21.

20. Noppeney U, Friston KJ, Ashburner J, Frackowiak R, Price CJ. Early visual deprivation induces structural plasticity in gray and white matter. Curr Biol. 2005 Jul;15(13):R488–90.

21. Noppeney U. The effects of visual deprivation on functional and structural organization of the human brain. Neurosci Biobehav Rev. 2007;31(8):1169–80.

22. Pascual-Leone A, Amedi A, Fregni F, Merabet LB. The plastic human brain cortex. Annu Rev Neurosci. 2005 Jul;28(1):377–401.

23. Burton H. Visual cortex activity in early and late blind people. J Neurosci. 2003 May;23(10):4005–11.

24. Bedny M, Pascual-Leone A, Dodell-Feder D, Fedorenko E, Saxe R. Language processing in the occipital cortex of congenitally blind adults. Proc Natl Acad Sci. 2011 Mar;108(11):4429–34.

25. Voss P, Zatorre RJ. Organization and reorganization of sensory-deprived cortex. Curr Biol. 2012 Mar;22(5):R168–73.

26. Gudi-Mindermann H, Rimmele JM, Nolte G, Bruns P, Engel AK, Roeder B. Working memory training in congenitally blind individuals results in an integration of occipital cortex in functional networks. Behav Brain Res. 2018 Aug;348:31–41.

27. Elbert T, Sterr A, Rockstroh B, Pantev C, Müller MM, Taub E. Expansion of the tonotopic area in the auditory cortex of the blind. J Neurosci. 2002 Nov;22(22):9941–4.

28. Roeder B, Roesler F, Hennighausen E, Nicker F. Event-related potentials during auditory and somatosensory discrimination in sighted and blind human subjects. Cogn Brain Res. 1996 Feb;4:17.

29. Roeder B, Neville H. Developmental functional plasticity. Grafman J, Robertson I, editors. Handb Neuropsychol. 2003;(9):231–70.

30. Burton H, Snyder AZ, Raichle ME. Resting state functional connectivity in early blind humans. Front Syst Neurosci [Internet]. 2014 Apr [cited 2019 Mar 6];8. Available from: http://journal.frontiersin.org/article/10.3389/fnsys.2014.00051/abstract

31. Pelland M, Orban P, Dansereau C, Lepore F, Bellec P, Collignon O. State-dependent modulation of functional connectivity in early blind individuals. NeuroImage. 2017 Feb;147:532–41.

32. Klinge C, Eippert F, Roder B, Buchel C. Corticocortical Connections Mediate Primary Visual Cortex Responses to Auditory Stimulation in the Blind. J Neurosci. 2010 Sep 22;30(38):12798–805.

33. Liu Y, Yu C, Liang M, Li J, Tian L, Zhou Y, et al. Whole brain functional connectivity in the early blind. Brain. 2007 Aug;130(8):2085–96.

34. Yu C, Liu Y, Li J, Zhou Y, Wang K, Tian L, et al. Altered functional connectivity of primary visual cortex in early blindness. Hum Brain Mapp. 2008 May;29(5):533–43.

35. Buzsaki G. Neuronal oscillations in cortical networks. Science. 2004 Jun;304(5679):1926–9.

36. Buzsáki G, Logothetis N, Singer W. Scaling brain size, keeping timing: evolutionary preservation of brain rhythms. Neuron. 2013 Oct;80(3):751–64.

37. Singer W. Neuronal oscillations: unavoidable and useful? Eur J Neurosci. 2018 Oct;48(7):2389–98.

38. Keitel A, Gross J. Individual human brain areas can be identified from their characteristic spectral activation fingerprints. Engel AK, editor. PLOS Biol. 2016 Jun;14(6):e1002498.

39. Giraud A-L, Kleinschmidt A, Poeppel D, Lund TE, Frackowiak RSJ, Laufs H. Endogenous cortical rhythms determine cerebral specialization for speech perception and production. Neuron. 2007 Dec;56(6):1127–34.

40. Engel AK, König P, Kreiter AK, Schillen TB, Singer W. Temporal coding in the visual cortex: new vistas on integration in the nervous system. Trends Neurosci. 1992 Jun;15(6):218–26.

41. Singer W. Cortical dynamics revisited. Trends Cogn Sci. 2013 Dec;17(12):616–26.

42. Raichle ME. The restless brain. Brain Connect. 2011 Jan;1(1):3–12.

43. Hipp JF, Engel AK, Siegel M. Oscillatory synchronization in large-scale cortical networks predicts perception. Neuron. 2011 Jan;69(2):387–96.

44. Singer W, Gray CM. Visual feature integration and the temporal correlation hypothesis. 1995;32.

45. Engel AK, Fries P, Singer W. Dynamic predictions: Oscillations and synchrony in top–down processing. Nat Rev Neurosci. 2001 Oct;2(10):704–16.

46. Lakatos P, Karmos G, Mehta AD, Ulbert I, Schroeder CE. Entrainment of neuronal oscillations as a mechanism of attentional selection. Science. 2008 Apr;320(5872):110–3.

47. Holcombe AO. Seeing slow and seeing fast: two limits on perception. Trends Cogn Sci. 2009 May;13(5):216–21.

48. Giraud A-L, Poeppel D. Cortical oscillations and speech processing: emerging computational principles and operations. Nat Neurosci. 2012 Apr;15(4):511–7.

49. VanRullen R. Perceptual rhythms. In: Wixted JT, editor. Stevens' Handbook of Experimental Psychology and Cognitive Neuroscience [Internet]. Hoboken, NJ, USA: John Wiley & Sons, Inc.; 2018 [cited 2019 Jul 29]. p. 1–44. Available from: http://doi.wiley.com/10.1002/9781119170174.epcn212

50. Portoles O, Borst JP, van Vugt MK. Characterizing synchrony patterns across cognitive task stages of associative recognition memory. Eur J Neurosci. 2018 Oct;48(8):2759–69.

51. Schroeder SCY, Ball F, Busch NA. The role of alpha oscillations in distractor inhibition during memory retention. Eur J Neurosci. 2018 Oct;48(7):2516–26.

52. Lakatos P, Musacchia G, O'Connel MN, Falchier AY, Javitt DC, Schroeder CE. The Spectrotemporal Filter Mechanism of Auditory Selective Attention. Neuron. 2013 Feb;77(4):750–61.

53. Heusser AC, Poeppel D, Ezzyat Y, Davachi L. Episodic sequence memory is supported by a theta–gamma phase code. Nat Neurosci. 2016 Oct;19(10):1374–80.

54. Deco G, Jirsa VK, McIntosh AR. Emerging concepts for the dynamical organization of resting-state activity in the brain. Nat Rev Neurosci. 2011 Jan;12(1):43–56.

55. Raichle ME. The restless brain: how intrinsic activity organizes brain function. Philos Trans R Soc B Biol Sci. 2015 May;370(1668):20140172.

56. Engel AK, Gerloff C, Hilgetag CC, Nolte G. Intrinsic Coupling Modes: Multiscale Interactions in Ongoing Brain Activity. Neuron. 2013 Nov;80(4):867–86.

57. Sormaz M, Murphy C, Wang H, Hymers M, Karapanagiotidis T, Poerio G, et al. Default mode network can support the level of detail in experience during active task states. Proc Natl Acad Sci. 2018 Sep 11;115(37):9318–23.

58. De Luca M, Beckmann CF, De Stefano N, Matthews PM, Smith SM. fMRI resting state networks define distinct modes of long-distance interactions in the human brain. NeuroImage. 2006 Feb;29(4):1359–67.

59. de Pasquale F, Della Penna S, Snyder AZ, Lewis C, Mantini D, Marzetti L, et al. Temporal dynamics of spontaneous MEG activity in brain networks. Proc Natl Acad Sci. 2010 Mar;107(13):6040–5.

60. Adrian ED. The bebgee rhythm: potential changes from the occipital lobes in man. 1934;31.

61. Noebels JL, Roth WT, Kopell BS. Cortical slow potentials and the occipital EEG in congenital blindness. J Neurol Sci. 1978 Jun;37(1–2):51–8.

62. Kriegseis A, Hennighausen E, Roesler F, Roeder B. Reduced EEG alpha activity over parieto-occipital brain areas in congenitally blind adults. Clin Neurophysiol. 2006 Jul;117(7):1560–73.

63. Hawellek DJ, Schepers IM, Roeder B, Engel AK, Siegel M, Hipp JF. Altered intrinsic neuronal interactions in the visual cortex of the blind. J Neurosci. 2013 Oct;33(43):17072–80.

64. Schubert JTW, Buchholz VN, Foecker J, Engel AK, Roeder B, Heed T. Oscillatory activity reflects differential use of spatial reference frames by sighted and blind individuals in tactile attention. NeuroImage. 2015 Aug;117:417–28.

65. Schepers IM, Hipp JF, Schneider TR, Roeder B, Engel AK. Functionally specific oscillatory activity correlates between visual and auditory cortex in the blind. Brain. 2012 Mar;135(3):922–34.

66. Tzourio-Mazoyer N, Landeau B, Papathanassiou D, Crivello F, Etard O, Delcroix N, et al. Automated anatomical labeling of activations in SPM using a macroscopic anatomical parcellation of the MNI MRI single-subject brain. NeuroImage. 2002 Jan;15(1):273–89.

67. MacQueen J. Some methods for classification and analysis of multivariate observations. 1967 Jun;281–97.

68. Reynolds DA, Rose RC. Robust text-independent speaker identification using Gaussian mixture speaker models. IEEE Trans Speech Audio Process. 1995;3(1):72–83.

69. Smith SM, Jenkinson M, Johansen-Berg H, Rueckert D, Nichols TE, Mackay CE, et al. Tract-based spatial statistics: Voxelwise analysis of multi-subject diffusion data. NeuroImage. 2006 Jul;31(4):1487–505.

70. Thiebaut de Schotten M, ffytche DH, Bizzi A, Dell'Acqua F, Allin M, Walshe M, et al. Atlasing location, asymmetry and inter-subject variability of white matter tracts in the human brain with MR diffusion tractography. NeuroImage. 2011 Jan;54(1):49–59.

71. Rosanova M, Casali A, Bellina V, Resta F, Mariotti M, Massimini M. Natural Frequencies of Human Corticothalamic Circuits. J Neurosci. 2009 Jun 17;29(24):7679–85.

72. Ferrarelli F, Sarasso S, Guller Y, Riedner BA, Peterson MJ, Bellesi M, et al. Reduced Natural Oscillatory Frequency of Frontal Thalamocortical Circuits in Schizophrenia. Arch Gen Psychiatry [Internet]. 2012 Aug 1 [cited 2019 Sep 22];69(8). Available from: http://archpsyc.jamanetwork.com/article.aspx?doi=10.1001/archgenpsychiatry.2012.147

73. Striem-Amit E, Ovadia-Caro S, Caramazza A, Margulies DS, Villringer A, Amedi A. Functional connectivity of visual cortex in the blind follows retinotopic organization principles. Brain. 2015 Jun;138(6):1679–95.

74. Magrou L, Barone P, Markov NT, Killackey HP, Giroud P, Berland M, et al. How Areal Specification Shapes the Local and Interareal Circuits in a Macaque Model of Congenital Blindness. Cereb Cortex. 2018 Aug 1;28(8):3017–34.

75. Voss P. Brain (re)organization following visual loss. Wiley Interdiscip Rev Cogn Sci. 2019 Jan;10(1):e1468.

76. Haak KV, Beckmann CF. Plasticity versus stability across the human cortical visual connectome. Nat Commun. 2019 Dec;10(1):3174.

77. Ortiz-Terán L, Diez I, Ortiz T, Perez DL, Aragón JI, Costumero V, et al. Brain circuit–gene expression relationships and neuroplasticity of multisensory cortices in blind children. Proc Natl Acad Sci. 2017 Jun;201619121.

78. Goodale MA, Milner AD. Separate visual pathways for perception and action. Trends Neurosci. 1992 Jan;15(1):20–5.

79. Haegens S, Nacher V, Luna R, Romo R, Jensen O. Alpha-Oscillations in the monkey sensorimotor network influence discrimination performance by rhythmical inhibition of neuronal spiking. Proc Natl Acad Sci. 2011 Nov;108(48):19377–82.

80. Michalareas G, Vezoli J, van Pelt S, Schoffelen J-M, Kennedy H, Fries P. Alpha-beta and gamma rhythms subserve feedback and feedforward influences among human visual cortical areas. Neuron. 2016 Jan;89(2):384–97.

81. Popov T, Kastner S, Jensen O. FEF-controlled alpha delay activity precedes stimulus-induced gamma-Band activity in visual cortex. J Neurosci. 2017 Apr;37(15):4117–27.

82. Roeder B, Gudi-Mindermann H, Shareef I, Rimmele JM, Sourav S, Kekunnaya R, et al. Spectral profiles of resting state EEG in permanently congenital blind and sight recovery individuals. underRevision.

83. van Kerkoerle T, Self MW, Dagnino B, Gariel-Mathis M-A, Poort J, van der Togt C, et al. Alpha and gamma oscillations characterize feedback and feedforward processing in monkey visual cortex. Proc Natl Acad Sci. 2014 Oct;111(40):14332–41.

84. Schmiedt JT, Maier A, Fries P, Saunders RC, Leopold DA, Schmid MC. Beta oscillation dynamics in extrastriate cortex after removal of primary visual cortex. J Neurosci. 2014 Aug;34(35):11857–64.

85. Veraart C, De Volder AG, Wanet-Defalque MC, Bol A, Michel C, Goffinet AM. Glucose utilization in human visual cortex is abnormally elevated in blindness of early onset but decreased in blindness of late onset. Brain Res. 1990 Feb;510(1):115–21.

86. Wanet-Defalque M-C, Veraart C, De Volder A, Metz R, Michel C, Dooms G, et al. High metabolic activity in the visual cortex of early blind human subjects. Brain Res. 1988 Apr;446(2):369–73.

87. Bedny M. Evidence from blindness for a cognitively pluripotent cortex. Trends Cogn Sci. 2017 Sep;21(9):637–48.

88. Gross J, Hoogenboom N, Thut G, Schyns P, Panzeri S, Belin P, et al. Speech rhythms and multiplexed oscillatory sensory coding in the human brain. Poeppel D, editor. PLoS Biol. 2013 Dec;11(12):e1001752.

89. Rimmele JM, Gross J, Molholm S, Keitel A. Editorial: Brain oscillations in human communication. Front Hum Neurosci [Internet]. 2018 Feb [cited 2019 Jan 16];12. Available from: http://journal.frontiersin.org/article/10.3389/fnhum.2018.00039/full

90. Rimmele JM, Morillon B, Poeppel D, Arnal LH. Proactive Sensing of Periodic and Aperiodic Auditory Patterns. Trends Cogn Sci. 2018 Oct;22(10):870–82.

91. Dietrich S, Hertrich I, Ackermann H. Training of ultra-fast speech comprehension induces functional reorganization of the central-visual system in late-blind humans. Front Hum Neurosci [Internet]. 2013 [cited 2019 Feb 22];7. Available from: http://journal.frontiersin.org/article/10.3389/fnhum.2013.00701/abstract

92. Penn LR, Ayasse ND, Wingfield A, Ghitza O. The possible role of brain rhythms in perceiving fast speech: Evidence from adult aging. J Acoust Soc Am. 2018 Oct;144(4):2088–94.

93. Binder JR, Desai RH, Graves WW, Conant LL. Where Is the Semantic System? A Critical Review and Meta-Analysis of 120 Functional Neuroimaging Studies. Cereb Cortex. 2009 Dec;19(12):2767–96.

94. Dehaene-Lambertz G, Montavont A, Jobert A, Allirol L, Dubois J, Hertz-Pannier L, et al. Language or music, mother or Mozart? Structural and environmental influences on infants' language networks. Brain Lang. 2010 Aug;114(2):53–65.

95. Vigneau M, Beaucousin V, Hervé PY, Duffau H, Crivello F, Houdé O, et al. Meta-analyzing left hemisphere language areas: Phonology, semantics, and sentence processing. NeuroImage. 2006 May;30(4):1414–32.

96. Friederici AD. Towards a neural basis of auditory sentence processing. Trends Cogn Sci. 2002 Feb;6(2):78–84.

97. Roeder B, Stock O, Bien S, Neville H, Roesler F. Speech processing activates visual cortex in congenitally blind humans: Plasticity of language functions in blind adults. Eur J Neurosci. 2002 Sep;16(5):930–6.

98. Lane C, Kanjlia S, Richardson H, Fulton A, Omaki A, Bedny M. Reduced left lateralization of language in congenitally blind individuals. J Cogn Neurosci. 2017 Jan;29(1):65–78.

99. Weiss S, Mueller HM. "Too Many betas do not Spoil the Broth": The Role of Beta Brain Oscillations in Language Processing. Front Psychol [Internet]. 2012 [cited 2019 Oct 25];3. Available from: http://journal.frontiersin.org/article/10.3389/fpsyg.2012.00201/abstract

100. Catani M, Mesulam M. The arcuate fasciculus and the disconnection theme in language and aphasia: History and current state. Cortex. 2008 Sep;44(8):953–61.

101. Hofstetter S, Sabbah N, Mohand-Saïd S, Sahel J-A, Habas C, Safran AB, et al. The development of white matter structural changes during the process of deterioration of the visual field. Sci Rep. 2019 Dec;9(1):2085.

102. Restani L, Caleo M. Reorganization of Visual Callosal Connections Following Alterations of Retinal Input and Brain Damage. Front Syst Neurosci [Internet]. 2016 Nov 14 [cited 2019 Nov 15];10. Available from: http://journal.frontiersin.org/article/10.3389/fnsys.2016.00086/full

103. Van Veen BD, Van Drongelen W, Yuchtman M, Suzuki A. Localization of brain electrical activity via linearly constrained minimum variance spatial filtering. IEEE Trans Biomed Eng. 1997 Sep;44(9):867–80.

104. Rousseeuw PJ. Silhouettes: A graphical aid to the interpretation and validation of cluster analysis. J Comput Appl Math. 1987 Nov;20:53–65.

105. Jenkinson M, Beckmann CF, Behrens TEJ, Woolrich MW, Smith SM. FSL. NeuroImage. 2012 Aug;62(2):782–90.

106. Smith SM. Fast robust automated brain extraction. Hum Brain Mapp. 2002 Nov;17(3):143–55.

107. Song S-K, Sun S-W, Ramsbottom MJ, Chang C, Russell J, Cross AH. Dysmyelination Revealed through MRI as Increased Radial (but Unchanged Axial) Diffusion of Water. NeuroImage. 2002 Nov;17(3):1429–36.

108. Song S-K, Yoshino J, Le TQ, Lin S-J, Sun S-W, Cross AH, et al. Demyelination increases radial diffusivity in corpus callosum of mouse brain. NeuroImage. 2005 May;26(1):132–40.

109. Klawiter EC, Schmidt RE, Trinkaus K, Liang H-F, Budde MD, Naismith RT, et al. Radial diffusivity predicts demyelination in ex vivo multiple sclerosis spinal cords. NeuroImage. 2011 Apr;55(4):1454–60.

110. Zatorre RJ, Fields RD, Johansen-Berg H. Plasticity in gray and white: neuroimaging changes in brain structure during learning. Nat Neurosci. 2012 Apr;15(4):528–36.

111. Aung WY, Mar S, Benzinger TL. Diffusion tensor MRI as a biomarker in axonal and myelin damage. Imaging Med. 2013 Oct;5(5):427–40.

112. Andersson JLR, Jenkinson M, Smith S. Non-linear registration, aka spatial normalisation. FMRIB Technial Report TR07JA2. (Oxford Centre for Functional Magnetic Resonance Imaging of the Brain, Department of Clinical Neurology, Oxford University). 2007;62.

113. Smith S, Nichols T. Threshold-free cluster enhancement: Addressing problems of smoothing, threshold dependence and localisation in cluster inference. NeuroImage. 2009 Jan 1;44(1):83–98.

114. Nichols TE, Holmes AP. Nonparametric permutation tests for functional neuroimaging: A primer with examples. Hum Brain Mapp. 2002 Jan;15(1):1–25.